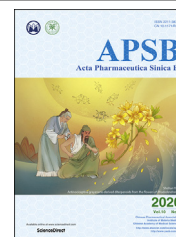




Chinese Pharmaceutical Association
Institute of Materia Medica, Chinese Academy of Medical Sciences

Acta Pharmaceutica Sinica B

www.elsevier.com/locate/apsb
www.sciencedirect.com



ORIGINAL ARTICLE

The construction of *in vitro* nasal cavity-mimic M-cell model, design of M cell-targeting nanoparticles and evaluation of mucosal vaccination by nasal administration



Xiaotong Yang^{a,†}, Xianchun Chen^{b,†}, Ting Lei^a, Lin Qin^a, Yang Zhou^a,
Chuan Hu^a, Qingfeng Liu^{c,*}, Huile Gao^{a,*}

^aKey Laboratory of Drug Targeting and Drug Delivery System of the Education Ministry, Sichuan Engineering Laboratory for Plant-Sourced Drug and Sichuan Research Center for Drug Precision Industrial Technology, West China School of Pharmacy Sichuan University, Chengdu 610041, China

^bCollege of Materials Science and Engineering, Sichuan University, Chengdu 610064, China

^cShanghai University of Medicine & Health Sciences Affiliated Sixth People's Hospital South Campus, Shanghai 201499, China

Received 7 January 2020; received in revised form 13 February 2020; accepted 16 February 2020

KEY WORDS

M cells;
In vitro;
Cell model;
iRGD peptide;
Nasal administration;
Mucosal vaccination

Abstract In order to better evaluate the transport effect of nanoparticles through the nasal mucosa, an *in vitro* nasal cavity-mimic model was designed based on M cells. The differentiation of M cells was induced by co-culture of Calu-3 and Raji cells in invert model. The ZO-1 protein staining and the transport of fluorescein sodium and dexamethasone showed that the inverted co-culture model formed a dense monolayer and possessed the transport ability. The differentiation of M cells was observed by up-regulated expression of Sialyl Lewis A antigen (SLAA) and integrin $\beta 1$, and down-regulated activity of alkaline phosphatase. After targeting M cells with iRGD peptide (cRGDKGPDC), the transport of nanoparticles increased. *In vivo*, the co-administration of iRGD could result in the increase of nanoparticles transported to the brain through the nasal cavity after intranasal administration. In the evaluation of immune effect *in vivo*, the nasal administration of OVA-PLGA/iRGD led to more release of IgG, IFN- γ , IL-2 and secretory IgA (sIgA) compared with OVA@PLGA group. Collectively, the study constructed

*Corresponding authors.

E-mail addresses: 155135562@qq.com (Qingfeng Liu), gaohuile@scu.edu.cn (Huile Gao).

[†]These authors made equal contributions to this work.

Peer review under responsibility of Chinese Pharmaceutical Association and Institute of Materia Medica, Chinese Academy of Medical Sciences.

<https://doi.org/10.1016/j.apsb.2020.02.011>

2211-3835 © 2020 Chinese Pharmaceutical Association and Institute of Materia Medica, Chinese Academy of Medical Sciences. Production and hosting by Elsevier B.V. This is an open access article under the CC BY-NC-ND license (<http://creativecommons.org/licenses/by-nc-nd/4.0/>).

in vitro M cell model, and proved the enhanced effect of targeting towards M cell with iRGD on improving nasal immunity.

© 2020 Chinese Pharmaceutical Association and Institute of Materia Medica, Chinese Academy of Medical Sciences. Production and hosting by Elsevier B.V. This is an open access article under the CC BY-NC-ND license (<http://creativecommons.org/licenses/by-nc-nd/4.0/>).

1. Introduction

Nasal administration typically delivers drug through the absorption from nasal mucosa to blood circulation and other tissue to exert a local or systemic therapeutic effect. Compared with other administration routes, nasal administration exhibits some unparalleled advantages, such as its rapid absorption, the avoidance of first-pass effect in the liver, high bioavailability, and direct entry into brain, etc^{1–5}. Nasal administration is especially promising in vaccine immunity, due to the existence of nasal mucosa-related lymphoid tissue, which contains abundant immune cells, such as B cells, CD4⁺ and CD8⁺ lymphocytes, and dendritic cells^{6–10}. After the uptake and delivery of antigen *via* M cells, the antigens are immediately processed and presented by dendritic cells. Mucosal lymphocytes then emigrate from the nasal-associated lymphoid tissue (NALT), circulate through the bloodstream and home to distant mucosal effector sites to induce immune response. Compared with intramuscular and subcutaneous injections, nasal administration can stimulate not only the systemic immunity, but the mucosal immune response, resulting in more complete immune protection^{11–13}.

Due to enzyme degradation when exposed to the nasal environment, nano delivery system is adopted for the nasal administration to improve the stability of immunogens. Therefore, simple and effective *in vitro* evaluation model is urgently needed for nasal preparation to conduct various studies on the nasal absorption, metabolic characteristics and toxicity of the drug delivery system. The *in vitro* models are often presented by isolating primary mucosal epithelial cells or using a type of nasal epithelial cancer cell line^{14–16}, but these models cannot mimic the overall nasal mucosa due to the complexity of the nasal environment.

An in-depth study of the nasal mucosa revealed that M cells, distributed in the nasal mucosa, play a critical role in the translocation of antigen and drug, which is similar to that found in the Payer's Patch of intestinal epithelium^{17–19}. M cells are characterized by irregular shape and an absent brush border. Basolateral membrane of M cells is deeply caved, with a pocket-like shape to host some lymphocytes^{20,21}. Given that structure of M cells, nanoparticles and antigens have easier access to M cells rather than other cells in nasal mucosa. Therefore, the establishment of an *in-vitro* nasal model based on M cell differentiation can more accurately simulate the drug transport in the nasal mucosa.

To date, the *in vitro* M cell model has been obtained by co-culturing Raji lymphoma cells and Caco-2 colon cancer cells to induce differentiation of M cells^{22–25}. Moreover, the researchers improved the M-cell induction efficiency by developing the inverted co-culture model^{26,27}. However, this model is still not suitable for *in vitro* evaluation of nasal administration, mainly because Caco-2 cells lack the function of secreting mucus and expression of some ion channels, which is quite different from the physiological state of nasal cavity. Therefore, we chose to replace Caco-2 cells with Calu-3 cells to construct a nasal M cell model built on the inverted co-culture model. Apart from the properties

of forming polar monolayer membrane and tight junctions similar to Caco-2 cells, Calu-3 cells possess mucus-secreting ability so that this M cells model should better reflect the true state of the nasal M cells^{28–31}.

The outstanding characteristic of M cells is that they can efficiently transport macromolecule drugs or particles. However, the low distribution ratio of M cells limits the transport efficiency. Thus, it is of profound significance to design an M cell-targeting delivery system. Noting that some specific receptors overexpressed on M cells, such as α -L-fucose^{32,33}, claudin 4 protein and integrin β 1^{34–36}, ligand-modified nanoparticles have proved the targeting ability toward M cells (for instance, *Aleuria aurantia* lectin, CKS9 peptide and RGD)^{20,37–40}. Yet, complicated preparation still remains an inevitable challenge to be addressed. iRGD, as a cell membrane penetrating peptide, can bind to the α_v integrin receptor expressed on the cell surface by the contained RGD motif to promote the nanoparticle uptake *via* co-administration^{41,42}. M cells in intestinal mucosa were found to express integrin α_v receptor on the surface, which is essential for invasion of some pathogens⁴³. Therefore, we speculated that the co-administration of iRGD could combine with integrin receptor on the surface of M cells and promote the uptake of nanoparticles or antigens.

In this study, the co-culture inverted model of Calu-3 and Raji cells was established to evaluate the nasal transport and mechanism of nanoparticles. In addition, the targeting effects of iRGD were evaluated at the cellular and animal level. M cell-targeting enhanced the immune response of nasal administration, as proved by *in vivo* immune experiment. The research will provide an alternative model for *in vitro* evaluation of nasal delivery system, and help promote the further development of nasal delivery system.

2. Materials and methods

2.1. Materials

NH₂-PEG-SH (MW = 3400) was purchased from Laysan Bio, Inc. (Arab, USA). Bilirubin was purchased from Tokyo Chemical Industry Co., Ltd. (Tokyo, Japan). Albumin from chicken egg white lyophilized powder (\geq 98%) and poly (vinyl alcohol) (PVA) were purchased from Sigma-Aldrich Inc. (St. Louis, USA). Poly (D,L-lactide-co-glycolide) polymer (PLGA-50:50; inherent viscosity 0.55–0.75 dL/g) was purchased from LAC-TEL Absorbable Polymers (Birmingham, USA). The Bradford protein assay kit, BCA protein assay kit and Alkaline Phosphatase assay kit were purchased from Beyotime Biotechnology (Shanghai, China). iRGD was synthesized by Shanghai Dechi Biosciences Co., Ltd. (Shanghai, China). Coumarin-6, fluorescein sodium, dexamethasone, propranolol, chlorpromazine, filipin, sodium azide, and nocodazole were purchased from Dalian Meilun Biotech Co., Ltd. (Dalian, China). Matrigel™ Basement Membrane Matrix was obtained from Becton, Dickinson and

Company (Franklin Lakes, USA). Anti-ZO-1 tight junction protein antibody and anti-integrin $\beta 1$ antibody were purchased from Abcam (Cambridge, UK). CA19-9 monoclonal antibody was gained from Thermo Fisher Scientific (Waltham, USA). Human lung adenocarcinoma cell line (Calu-3) and lymphoma cell line (Raji) were purchased from the Chinese Academy of Science cells Bank (Shanghai, China).

Female BALB/c mice (18 ± 2 g) and Sprague–Dawley rats (150–200 g) were purchased from Dashuo Biotechnology Co., Ltd. (Chengdu, China). All animal experiments were performed under the guidelines approved by the Experiment Animal Administrative Committee of Sichuan University (Chengdu, China).

2.2. Construction of an *in vitro* M cell model

The normally oriented M cell model was obtained following the protocol as mentioned in the literature²⁶. Simply, 12-well transwell inserts were precoated with 300 μL /well Matrigel™ Basement Membrane Matrix, which were diluted in pure DMEM into a final protein concentration of 100 $\mu\text{g}/\text{mL}$, and placed in carbon dioxide cell culture chamber. After 1 h, the remaining liquid was removed and each transwell was washed with preheated 500 μL DMEM +1% (v/v) PEST. Then, Calu-3 cells were seeded on the upper side of insert at a density of 5×10^5 cells per well and cultured. After 7 days, Raji cells were suspended in DMEM+1% (v/v) PEST, and added to the basolateral side of insert about 5×10^5 cells per well. The co-cultures situation was lasted for 4–5 days. The upper chamber medium was replaced every two days. For the inverted model, the inserts were inverted after seeding Calu-3 cells for 3–5 days. A 1.5 cm-long silicone tube was placed at the end of the insert and filled with 500 μL medium. After another 5-day incubation, Raji cells were co-cultured in the basolateral compartment at same cell density as above. Five days later, the models were ready for use. The inverted mono-culture of Calu-3 cells was set as control.

2.3. Measurement of transepithelial electrical resistance (TEER)

TEER was measured every two days during the construction of cell model culture. Briefly, cell monolayers were washed twice in Hank's Balanced Salt Solution (HBSS), and filled with preheated medium. After 15–30 min of equilibration in the incubator, the TEER was measured by Millicell-ERS ohmmeter (Millipore, Boston, USA). The resistance of the cell culture insert without cells was considered as blank resistance and subtracted. The change in transmembrane resistance during cell growth was recorded.

2.4. Verifying the expression of ZO-1 protein

The cells were fixed in 4% paraformaldehyde for 20 min, washed with PBS for 3 times, and then blocked with 10% goat serum for 2 h. Then the rabbit anti-humanZO-1 antibody was diluted and incubated with cells at 4 °C for 12 h. The cells were washed 3 times with PBS, and incubated with Cy3-labeled donkey anti-rabbit secondary antibody for 2 h. After washing 3 times with PBS, the cells were stained with 0.5 $\mu\text{g}/\text{mL}$ DAPI for 5 min, and the pieces were observed by confocal microscopy (A1R+, Nikon, Tokyo, Japan). Sialyl Lewis A

antigen (SLAA) and integrin $\beta 1$ were stained and observed by the same method.

2.5. Transportation of sodium fluorescein and dexamethasone

Sodium fluorescein and dexamethasone were formulated into a final concentration of 500 $\mu\text{g}/\text{mL}$ and 1 mg/mL in HBSS, respectively. Take 100 μL of sodium fluorescein or dexamethasone solution into the apical chamber of M-cell model, and 600 μL of HBSS into basolateral chamber. Then, the plate was placed in a cell culture incubator. At 0.5, 1 and 2 h, 100 μL of liquid was sampled from the basolateral chamber and the same volume of blank HBSS was added. The concentrations of sodium fluorescein and dexamethasone were measured to calculate the apparent permeability coefficient [P_{app} , Eq. (1)]. The fluorescence intensity of sodium fluorescein was measured with microplate reader (Thermo Scientific Varioskan Flash, Waltham, USA) at an Ex/Em of 480 nm/530 nm. The dexamethasone was detected by high performance liquid chromatography (HPLC, Shimadzu, Kyoto, Japan). The mobile phase consisted of acetonitrile and water (45:55). The eluent was monitored at 240 nm. The flow rate was 1.0 mL/min and the column temperature was 40 °C.

$$P_{\text{app}} = (dQ/dt) / (A \times C_0) \quad (1)$$

where dQ/dt is the drug transport amount per unit time ($\mu\text{g}/\text{s}$); A is the area of the transport membrane (1.12 cm^2 for each well of 6-well plate, and 0.33 cm^2 for 12-well plate); C_0 is the initial concentration of sodium fluorescein or dexamethasone.

2.6. Detection of alkaline phosphatase activity

The medium in the apical and basolateral chamber was collected and centrifuged at $3000 \times g$ for 10 min, and the supernatant was taken and detected with an alkaline phosphatase activity kit. At the same time, the sample was used to quantify the protein concentration by BCA kit, and the enzyme activity/mg protein was calculated to compare the alkaline phosphatase activity of the monolayer membrane and the co-culture membrane.

2.7. Quantitative analysis of Raji cells on co-culture membrane

According to the description in the literature²⁶, Raji cells were labeled yellow–green fluorescent with a Cell Trace™ CFSE Cell Proliferation Kit according to the instructions at 3 days before co-cultures. Briefly, Cell Trace™ CFSE stock solution was diluted in PBS to 10 $\mu\text{mol}/\text{L}$, and prewarmed in 37 °C. Raji cells were collected, suspended in prepared solution at a density of 10×10^6 cells per tube and incubated at 37 °C. After 15 min, the cells were centrifuged and suspended in fresh prewarmed medium, and then incubated for another 30 min and washed. Three days later, CFSE-labeled Raji cells were cocultured with Calu-3 monolayer. After 5 days, the co-cultured cells were detected by flow cytometry (Becton, Dickinson and Company, Franklin Lakes, USA).

2.8. Model markers transportation evaluation

Propranolol and albumin were formulated into 10 $\mu\text{g}/\text{mL}$ and 2 mg/mL solution in HBSS, respectively. The method of the transport experiment is the same as that of previous transport experiment of fluorescein sodium and dexamethasone. In albumin transportation, a group of inserts were pre-incubated with

2.5 mmol/L EGTA (dissolved in HBSS, pH 7.4) twice for 15 min at 37 °C. EGTA (2.5 mmol/L) was set up to open the tight connection. The concentration of propranolol was determined by HPLC, and the concentration of albumin was determined by Bradford protein assay kit.

2.9. Transportation of cou@BRNPs

Nanoparticles were prepared by solvent diffusion method as described in the literature⁴⁴. The amphiphilic compounds formed by conjugation of bilirubin and PEG (Br-PEG) were synthesized. Afterwards, Br-PEG self-assembled in water to form micelles to carry hydrophobic molecules in the core (BRNPs). Briefly, coumarin-6 (10 µL, 10 mg/mL) was mixed with Br-PEG (200 mg/mL, 20 µL). The mixture was dripped into 2 mL water and stirred for 10 min, then the solution was centrifuged (6000×g, 10 min) to remove unencapsulated coumarin-6 and concentrated by ultrafiltration to prepare a concentration of 50 µg/mL of nanoparticle solution. 300 µL of cou@BRNPs solution or cou@BRNPs with 4.33 µg/mL iRGD was added apically to the M-cell model, and 1 mL of blank HBSS was added to the lower chamber and the plate was placed into incubator. At 0.25, 0.5, 1 and 2 h, 100 µL of the liquid was taken out from the lower chamber and the same volume of blank HBSS was added. The concentration of nanoparticles was measured using a microplate reader (Thermo Scientific Varioskan Flash).

2.10. Transportation of cou@PLGA nanoparticles

PLGA and coumarin-6 were dissolved in dichloromethane as the organic phase, and 1% PVA was used as the aqueous phase. Two phases were mixed together, sonicated for 5 min, and then the organic phase was removed by rotary evaporation. The remaining liquid was washed and concentrated by ultrafiltration. Nanoparticles transportation experiments were carried out as described above.

2.11. Transportation mechanism of nanoparticles

Co-culture membranes were pre-incubated with clathrin-mediated endocytosis inhibitor chlorpromazine (10 µg/mL), caveola-dependent endocytosis inhibitor filipin (5 µg/mL), energy generation inhibitor sodium azide (NaN₃, 2.6 mg/mL), and microtubule inhibitor nocodazole (33 µmol/L) for 3 h at 37 °C. Incubation at 4 °C was used to evaluate the influence of energy generation inhibition. Then, the cells were incubated with cou@BRNPs for 1 h as described previously. The number of transported nanoparticles was measured.

2.12. In vivo distribution of nanoparticle

Cy5.5@PLGA nanoparticles were prepared using the same procedure as that of cou@PLGA. Female BALB/c mice were randomly divided into two groups, which were intranasally administered with Cy5.5@PLGA/iRGD and Cy5.5@PLGA, respectively, at identical Cy5.5 dose of 35 µg/kg and iRGD dose of 4 µmol/kg. Mice were sacrificed at 0.5, 2, 4, 8 and 12 h after administration, and the distribution of nanoparticles was observed by Lumina III imaging system (PerkinElmer, Waltham, USA). Subsequently, the brains were divided into olfactory bulb, cortex, striatum, hippocampus, thalamus, midbrain, cerebellum, and pons

for slice preparation. The slices were stained with DAPI, and the fluorescence distribution was observed by confocal microscopy (A1R+, Nikon).

2.13. Nasal immunity studies

OVA@PLGA nanoparticles were prepared by multiple emulsion method. Briefly, OVA was dissolved in 1% PVA solution to form water phase, PLGA was dissolved in dichloromethane to form organic phase, then the two phases were mixed in a volume ratio of 1:10, and W/O emulsion was obtained by probe ultrasonication for 8 min. Then the emulsion was added with 5% PVA with a volume ratio of 1:6 for another 8 min ultrasonication. The organic solvent was evaporated to obtain OVA@PLGA nanoparticles.

Female Sprague–Dawley rats weighting between 150 and 200 g were used for the immunization studies. Prior to the experiment, rats were anesthetized by intraperitoneal injection of 10% chloral hydrate and animals were divided into 5 groups (9 rats in each group) to receive the following treatments: PBS, OVA@PLGA, OVA@PLGA/iRGD and plain OVA were administered intranasally, while intramuscular injection of OVA@PLGA (OVA@PLGA-im) was set as control. The dose of OVA was 50 µg/animal, and all animals were immunized on Day 0 and 14. On Days 7, 14, 28, and 42 after administration, blood of the rats was collected, and the concentration of OVA-specific IgG in the serum was measured by Rat OVA-IgG ELISA kit (ZCi Bio, Shanghai, China). Saliva and vaginal washes were also collected for determination of secretory IgA (sIgA) content by rat OVA-sIgA ELISA kit. Saliva and vaginal wash were sampled according to the method described in the literature⁴⁵. At the end of the experiment, the rats were sacrificed and alveolar lavage fluid was collected for sIgA assay. Spleens were isolated and homogenized in tissue lysate reagents. The solution was centrifuged at 3000×g for 20 min, and the endogenous cytokines (IFN-γ and IL-2) in the supernatant were assayed using rat IFN-γ and IL-2 ELISA kits according to the manufacturer's instructions.

3. Results and discussion

3.1. Characterization of the inverted in vitro M-cell model

3.1.1. Evaluation of cell monolayer integrity

The inverted model was adopted to shorten the distance between the two kinds of cells, and make the Raji cells infiltrating into the compartment membrane and contacting with Calu-3 cells to better induce M cells. After co-culture, the number of Raji cells labeled by CFSE in the cell monolayer was detected by flow cytometry (Fig. 1A). In the normal orientated co-cultures, Raji cells on the cell layer were hardly detected. On the inverted co-cultures, approximately 0.89% of the fluorescent-labeled Raji cells were detected. It indicated that the inverted co-culture provided better contact conditions for M cell differentiation.

TEER was monitored during cell culture. The TEER of the cell monolayer began to grow after 3 days of culture, and the inverted mono-culture TEER reached equilibrium on the 10th day (Fig. 1B). After starting co-cultivation, the inverted co-culture TEER value no longer increased and kept in the range of 250–340 Ω·cm². In general, TEER greater than 300 Ω·cm² is considered to be suitable for transport experiments⁴⁶. The relatively lower TEER than mono-cultures may be due to changes in

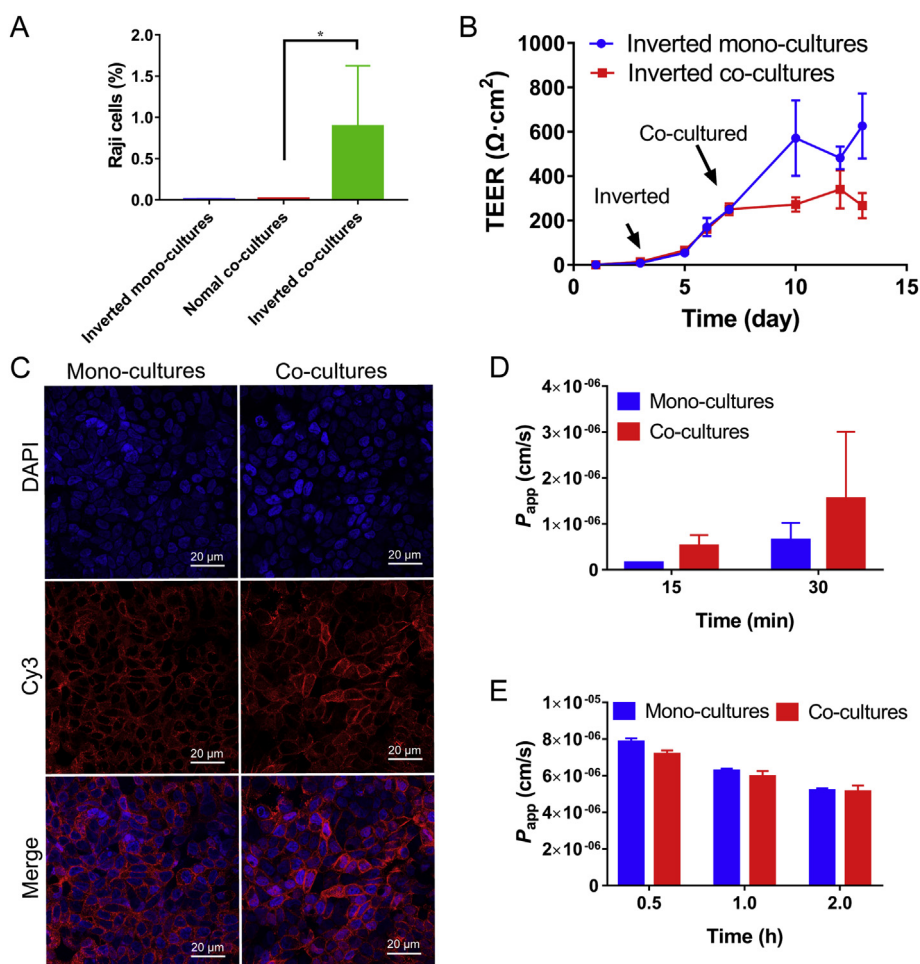


Figure 1 (A) Raji cells in the monolayers were calculated by flow cytometry analysis (means \pm SD, $n = 3$, $^*P < 0.05$). (B) The change of TEER in the culture progress (mean \pm SD, $n = 3$). (C) Confocal observation of ZO-1 in mono- and co-cultures. Cell nuclei were marked with DAPI (blue). Red fluorescence indicated the ZO-1 proteins. The P_{app} of sodium fluorescein (D) and dexamethasone (E) in mono- and co-cultures at different time points (mean \pm SD, $n = 3$).

the cell growth environment after co-culture, or a decrease in TEER value was observed when Calu-3 cells differentiated into M cells²⁶. Moreover, the red fluorescence-labeled tight junction protein ZO-1 was wrapped around nucleus (blue, Fig. 1C), indicating the successful formation of tight junction in cell monolayer. Then the transportation of sodium fluorescein, a marker for the detection of paracellular leakage, was detected (Fig. 1D). The P_{app} of sodium fluorescein was higher for co-cultures than mono-cultures because the tight junction of co-cultures may not be as tight as the mono-cultures as former analysis. But the P_{app} values were both around the standard range of 2×10^{-7} – 7×10^{-7} cm/s in 15 min, indicating that both the co-cultures and the mono-cultures formed dense tight connection. In addition, the transportation of the trans-cellular marker dexamethasone was measured to detect the transportation capacity of the cell monolayer (Fig. 1E). As time elapsed from 0.5 to 2 h, the P_{app} of the co-cultures and the mono-cultures decreased, probably owing to the effect of the drug on cell viability. But within 2 h, the P_{app} was greater than 5×10^{-6} cm/s, demonstrating that the cell layer kept transport ability. Through the above results, it can be concluded that the co-cultured and mono-cultured cell monolayer formed a tight junction and had good transportability, and can be used for subsequent nanoparticle transportation evaluation.

3.1.2. Verification of the differentiation of M cells

The powerful antigen capture ability of M cells plays an important role in the passage of antigens through the epithelial cell model. Differentiation of M cells is an indicator of successful establishment of the nasal epithelial model. The down regulation of alkaline phosphatase is a feature of M cell differentiation^{47,48}. In the end of culture (Fig. 2A), the alkaline phosphatase activity in the co-culture medium showed a lower level compared to the control group both in the apical and basolateral side medium, indicating the presence of M cell differentiation in co-cultures. Other indicators of M cell differentiation are the up-regulation of the SLAA^{34,49} and integrin $\beta 1$ expression. In the immunofluorescence observation of SLAA expression and integrin $\beta 1$ (Fig. 2B and C), the fluorescence of SLAA and integrin $\beta 1$ in the co-cultures was stronger than mono-cultures. The mean fluorescence density of SLAA and integrin $\beta 1$ was counted (Fig. 2D). In co-culture group, the mean fluorescence density of SLAA was 1.14 times of that of monolayer, and the value of integrin $\beta 1$ was 1.32 times of that of monolayer, indicating the differentiation of the M cells in the co-cultures. The above results were also proved by scanning electron microscope (SEM) analysis (Fig. 2E). The mono-cultures and the normal orientated co-cultures showed dense microvilli on the

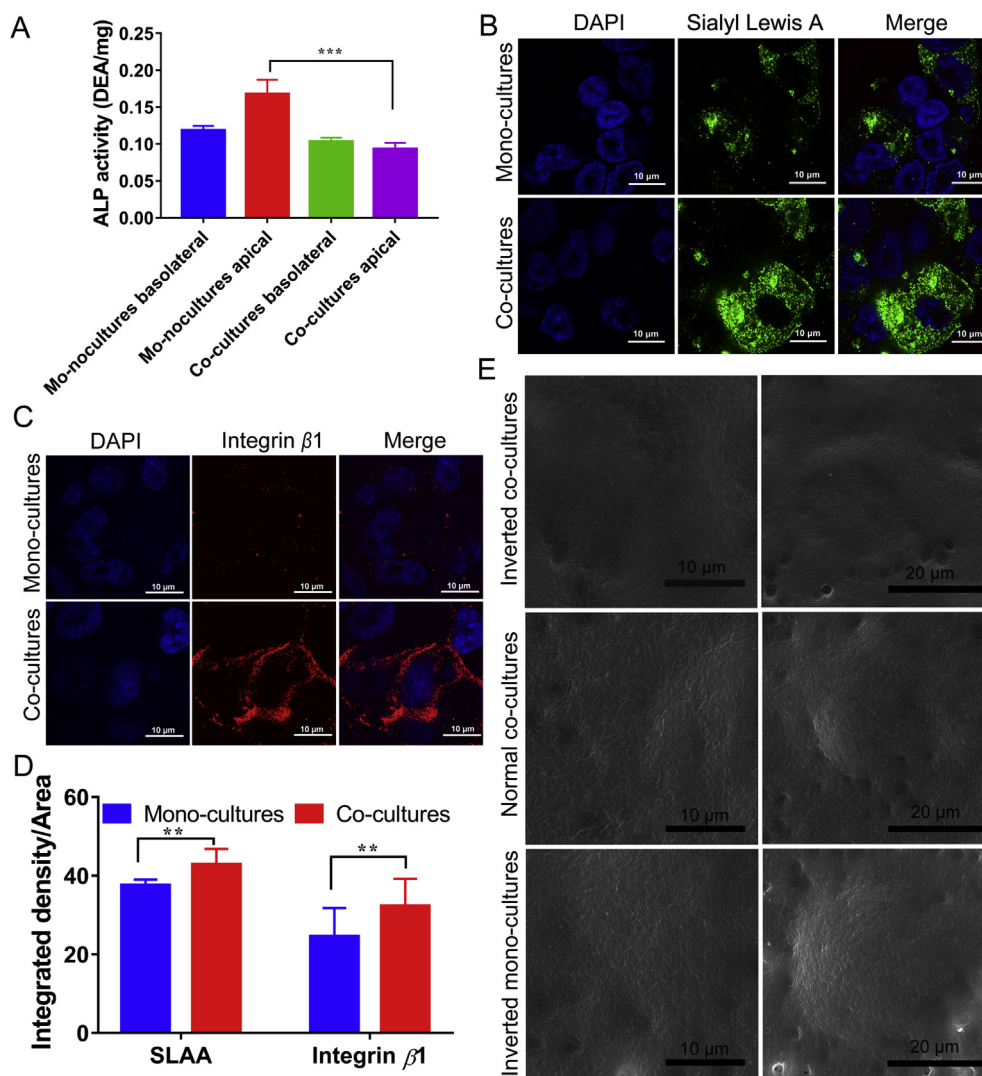


Figure 2 (A) The alkaline phosphatase activity in medium after culture (mean \pm SD, $n = 3$, *** $P < 0.001$). Confocal observation of Sialyl Lewis A antigen (B) and integrin $\beta 1$ (C) in mono- and co-cultures. The Sialyl Lewis A antigen was labeled with green fluorescence. The integrin $\beta 1$ was labeled with red fluorescence. Cell nucleus were marked with DAPI (blue). (D) Statistics of mean fluorescence density of Sialyl Lewis A antigen and integrin $\beta 1$ (mean \pm SD, $n = 3$, ** $P < 0.01$). (E) M cells were observed by SEM analysis.

surface of the cells, while a decreased number of microvilli were observed in inverted co-cultures, indicating that inverted co-culture effectively induced differentiation of M cells.

The outstanding feature of M cells is the efficient transport of macromolecules or nanoparticles. To analyze the role of M cells in nasal drug delivery, we evaluated the transport of different substances on the M cell model. Albumin was selected as a representative of macromolecular drug (Fig. 3A). The P_{app} of albumin was $1.30 \times 10^{-8} \pm 0.02 \times 10^{-8}$ cm/s in the co-cultures and $1.12 \times 10^{-8} \pm 0.18 \times 10^{-8}$ cm/s in mono-cultures. With the addition of 2.5 mmol/L EGTA, a calcium chelator to open tight junctions, the P_{app} of albumin in the co-cultures and mono-cultures were increased to $2.44 \times 10^{-8} \pm 0.01 \times 10^{-8}$ and $1.63 \times 10^{-8} \pm 0.05 \times 10^{-8}$ cm/s, respectively. The significant difference between the co-cultures and the mono-cultures may be due to the more loose tight junctions of co-cultures, or it may be due to the strong endocytosis caused by the differentiation of M cells. In a word, increased transport after EGTA addition confirmed the successful formation of tight junctions in cell

layers. Then, we chose high-absorbed small molecule propranolol as a representative of trans-cellular marker (Fig. 3B). The P_{app} of co-cultures and mono-cultures at 15 and 30 min were all around 8×10^{-6} cm/s, which were faster than that of albumin. It is worth indicating that there was no significant difference between co-cultures and mono-cultures, proving that the induction of M cells is more likely to influence the transportation of macromolecules.

3.2. *iRGD* promotes the transportation of nanoparticles

3.2.1. Transportation of nanoparticles with *iRGD* in M-cell model

M cells have strong antigen-capture capabilities. Nanoparticles with M cells-targeting ability will greatly increase transportation efficiency. The size of the cou@BRNPs was 116.4 ± 37.0 nm, measured by the dynamic light scattering (DLS, Fig. 3C). In the transportation experiment, the transportation speed of the co-cultures was faster than that of the mono-cultures, while the

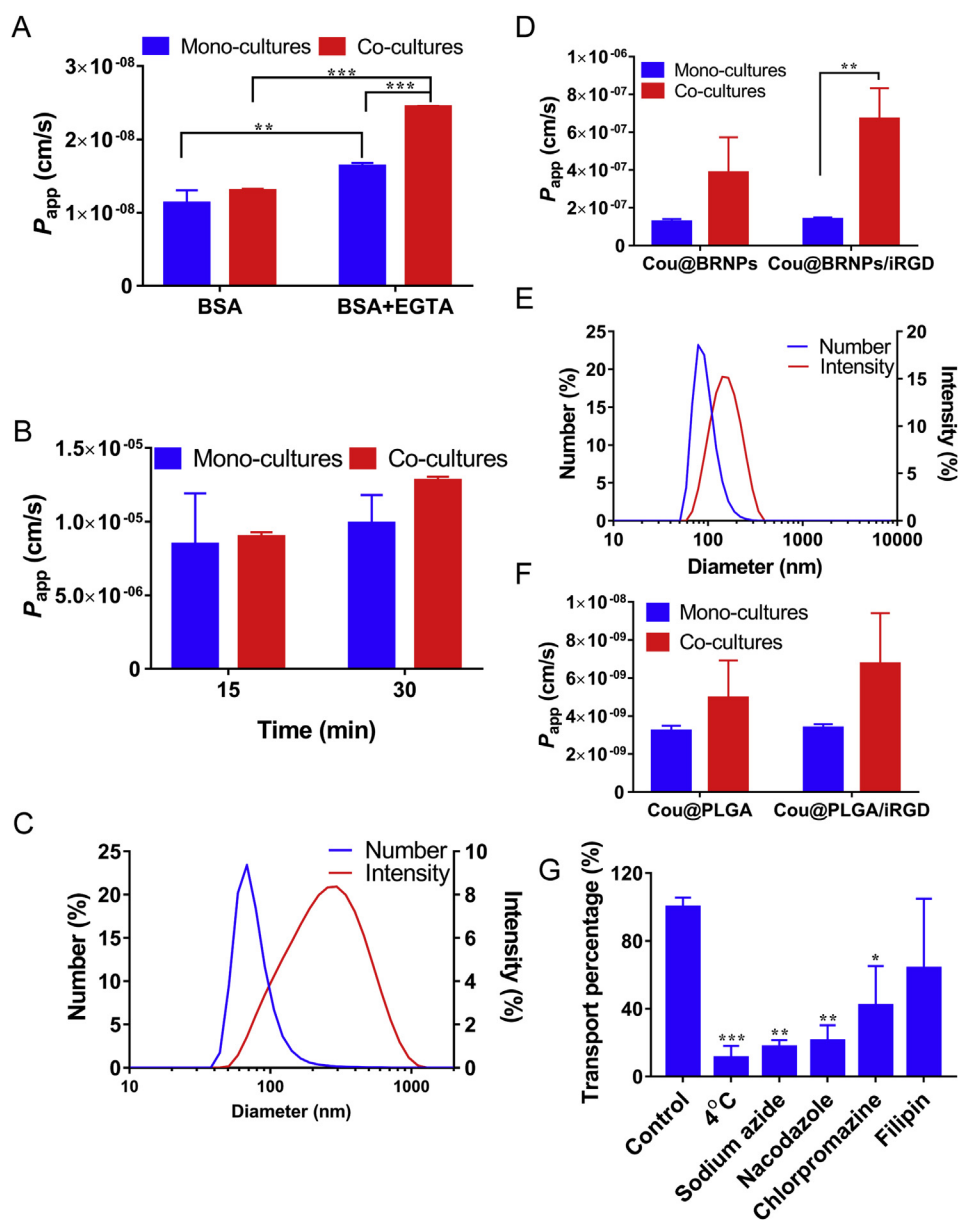


Figure 3 (A) The P_{app} of BSA with or without EGTA in mono- and co-cultures at transported for 1 h (mean \pm SD, $n = 3-8$, $**P < 0.01$, $***P < 0.001$). (B) The P_{app} of propranolol in mono- and co-cultures at transported for 15 and 30 min (mean \pm SD, $n = 3$). (C) Size distribution of cou@BRNPs by number and intensity. (D) The P_{app} of cou@BRNPs in mono- and co-cultures (mean \pm SD, $n = 3$). (E) Size distribution of cou@PLGA by number and intensity. (F) The P_{app} of cou@PLGA in mono- and co-cultures (mean \pm SD, $n = 3$). (G) The transport percentage calculated in the presence of inhibitors as compared with control (mean \pm SD, $n = 3$, $**P < 0.01$ and $***P < 0.001$ versus control group).

P_{app} of co-cultures was three times higher than that of mono-cultures (Fig. 3D). After co-administration of iRGD, the transportation was increased, and the P_{app} with iRGD in co-cultures was 1.7 times as high as that without iRGD, indicating that the iRGD could enhance the transportation of nanoparticles. Subsequently, the same experiment was performed with cou@PLGA nanoparticles, whose particle size was 99.4 ± 10.2 nm (Fig. 3E). After giving the iRGD, the transportation of nanoparticles in co-cultures was increased to 1.3 times of that without iRGD as expected (Fig. 3F). The above results suggested that iRGD increased the transportation of nanoparticles.

In order to study the transportation mechanism of nanoparticles in M cell model, different kinds of inhibitors were incubated with

the co-cultures during nanoparticle transport (Fig. 3G). Under the action of the energy inhibitor, sodium azide, the transportation percentage decreased to 17% of the control group, and transportation percentage at 4 °C decreased to 11% of the control, indicating that the transportation of nanoparticles was an energy-dependent progress. The transportation percentage of nacodazole group was only 21% of the control group, suggesting pinocytosis was involved in the transport progress. In addition, chlorpromazine inhibited about 59% nanoparticle transportation, indicating that the clathrin-mediated endocytosis was a transportation pathway of nanoparticles. In the filipin group, 36% nanoparticle transportation was inhibited, demonstrating the transport progress was also relevant to caveola-dependent endocytosis. These results

suggested that the transportation of the nanoparticles was a complex process, involving energy expenditure, clathrin-mediated endocytosis, and pinocytosis, etc.

3.2.2. *In vivo* verification of iRGD promoting nanoparticle transportation through nasal mucosa

To evaluate the effect of iRGD in promoting M cells uptake *in vivo*, live imaging was performed. After intranasal administration of Cy5.5@PLGA nanoparticles with a particle size of 66.3 ± 7.1 nm (Fig. 4A), the nanoparticles were ingested and distributed into the brain (Fig. 4B), mainly concentrating in the olfactory bulb, and reaching peak at 4 h. Compared with the control group, the fluorescence intensity of the iRGD group in the olfactory bulb was stronger than that of the control group. In the semi-quantitative results (Fig. 4C), the fluorescence intensity of

the iRGD group was 1.27 times higher than that of the control group at 4 h. Subsequently, the fluorescence distribution in frozen slices was observed (Fig. 4D) and the mean fluorescence density in different brain regions was counted (Fig. 4E), strong red fluorescence of nanoparticles was observed in the olfactory bulb, and the cerebral cortex was second to that of the olfactory bulb. In the striatum, hippocampus and other parts, the fluorescence was relatively weak. In addition, the fluorescence density of nanoparticles in olfactory bulb and cerebral cortex was higher than that in the control group after iRGD administration. It indicated that the iRGD could enhance the transportation of nanoparticles from the nasal cavity to the brain.

In addition, the nasal cavity of mice was divided into four parts to observe the distribution of nanoparticles in different depths of nasal mucosa (Fig. 5A). In the shallow parts (I and II), all

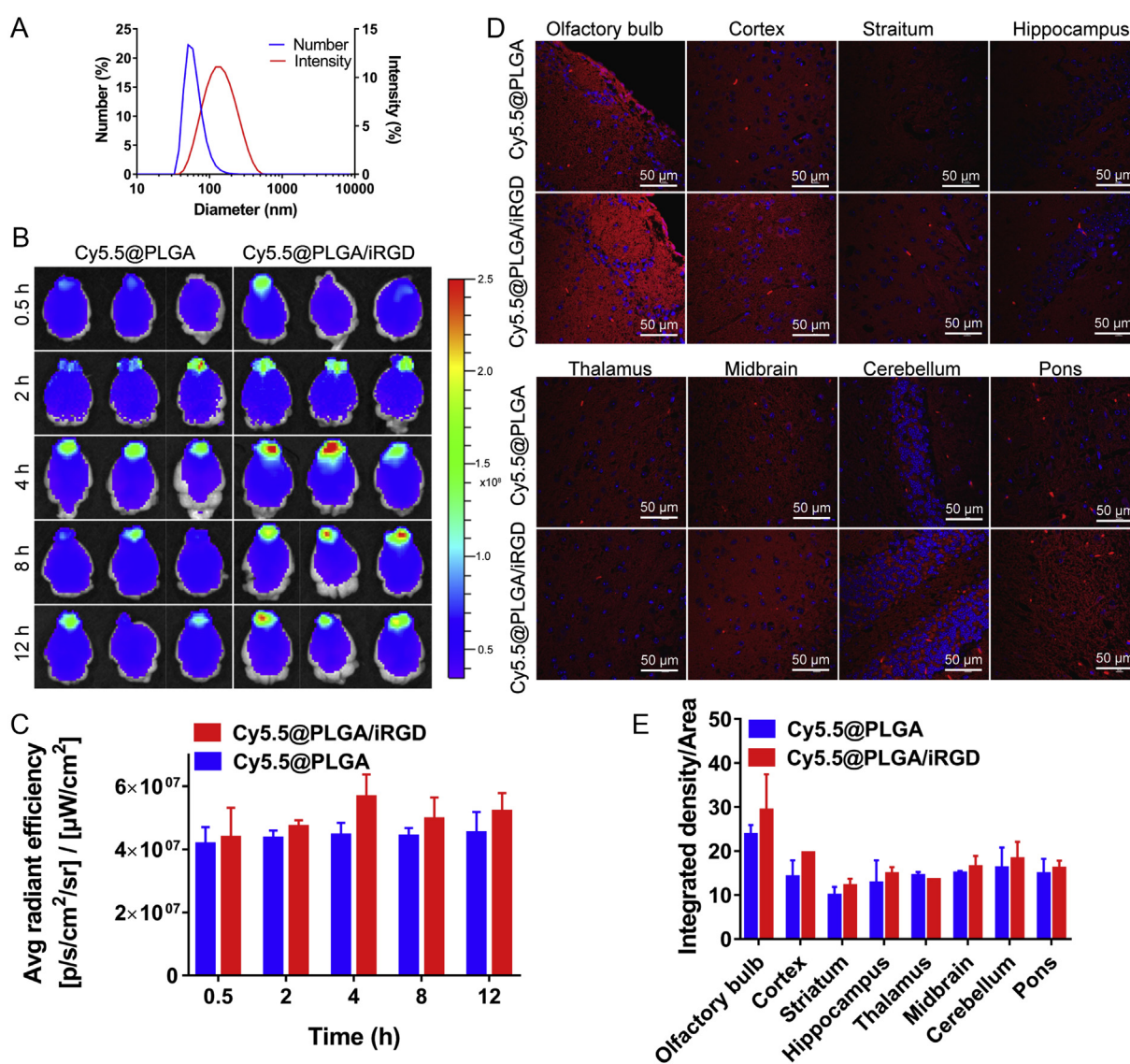


Figure 4 (A) Size distribution of Cy5.5@PLGA by number and intensity. (B) The distribution of Cy5.5@PLGA in mice brain. The fluorescent images were observed at different time post nanoparticles administration by living imaging. (C) Semi-quantitative data of fluorescence intensity in isolated brains (means \pm SD, $n = 3$). (D) Distribution of nanoparticles in different brain regions after 4 h administration. Cell nuclei were stained with DAPI (blue), and red signal indicated the nanoparticles. (E) Statistics of mean fluorescence density of nanoparticles in different brain regions (means \pm SD, $n = 3$).

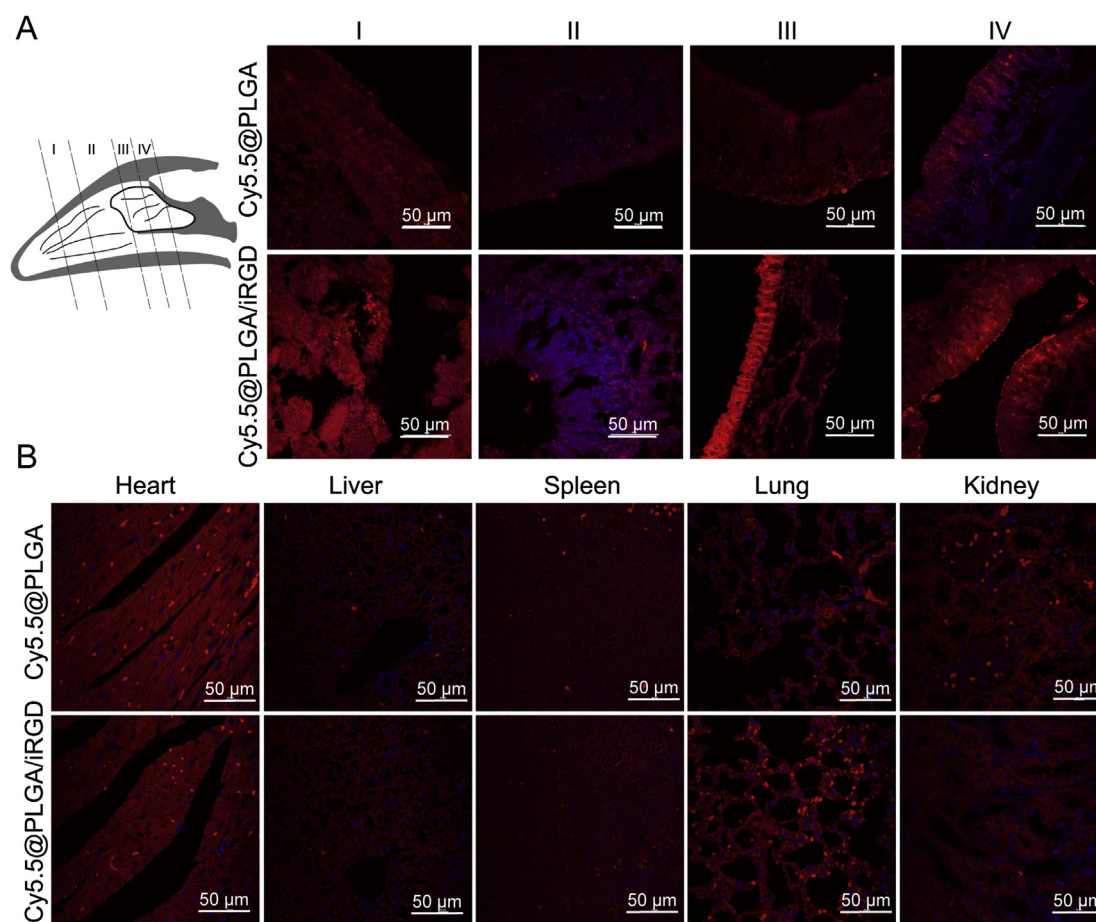


Figure 5 (A) Distribution of nanoparticles in different regions of nasal cavity according to the schematic. (B) Distribution of nanoparticles in frozen tissue sections observed by confocal microscopy. Red signal indicated the nanoparticles and the blue one was nucleus stained with DAPI.

nanoparticle fluorescence was weak. In the deep part of the nasal cavity (III and IV), there was higher nanoparticles distribution of the iRGD group compared with the control group. It was suggested that the application of iRGD may promote the uptake of nanoparticles in the nasal mucosa. Moreover, weak distribution of nanoparticles in the organs (including heart, liver, spleen, lung and kidney) were observed (Fig. 5B). That meant the part of nanoparticles entered the blood circulation and distributed throughout the body.

3.3. iRGD enhancing *in vivo* immunity of intranasal administration of OVA@PLGA

Nasal administration was a better mode of administration that stimulated mucosal immunity. In order to verify the enhanced effect of nasal mucosal immunity after iRGD co-administration, *in vivo* immune evaluation was carried out. OVA@PLGA nanoparticles were prepared in advance. The number size was 144.12 ± 12.54 nm, and the drug-loading capacity of the nanoparticles was determined to be 3.75% (Fig. 6A).

To investigate the immune effect of various formulations *in vivo*, serum collected from rats was used to detect the content of IgG. As shown in Fig. 6B, there was no obvious change in IgG

concentration at Days 7 and 14. At Day 42, the level of IgG in plain OVA nasal administration group and OVA@PLGA-im group did not increase significantly compared with the control group. While in the OVA@PLGA/iRGD group, the average IgG concentration was 1.34 times higher than that of the control group.

After nasal immunization with OVA@PLGA, B cells in nasal associated lymphoid tissue were activated and emigrated to bloodstream and home to the region of the respiratory and reproductive tracts. Then, secretory IgA (sIgA) + B cells terminally differentiate into IgA plasma cells for the generation of sIgA⁵⁰. As shown in Fig. 6C, the sIgA concentration of each group peaked at the 28th day. Compared with the control group, plain OVA and OVA@PLGA-im produced relatively weak immune response. The nasal administration of OVA@PLGA slightly increased. The highest concentration was provided by OVA@PLGA/iRGD group at different time points. The level of sIgA in OVA@PLGA/iRGD group was 1.94 times higher than OVA@PLGA group at Day 14, 1.64 times higher than OVA@PLGA group on Day 28, and 1.34 times higher than OVA@PLGA group on Day 42. At the same time, the sIgA level in the vaginal was measured (Fig. 6D), and the difference between each group and the control group was not obvious, while the iRGD group showed a weak advantage. The weak mucus immune

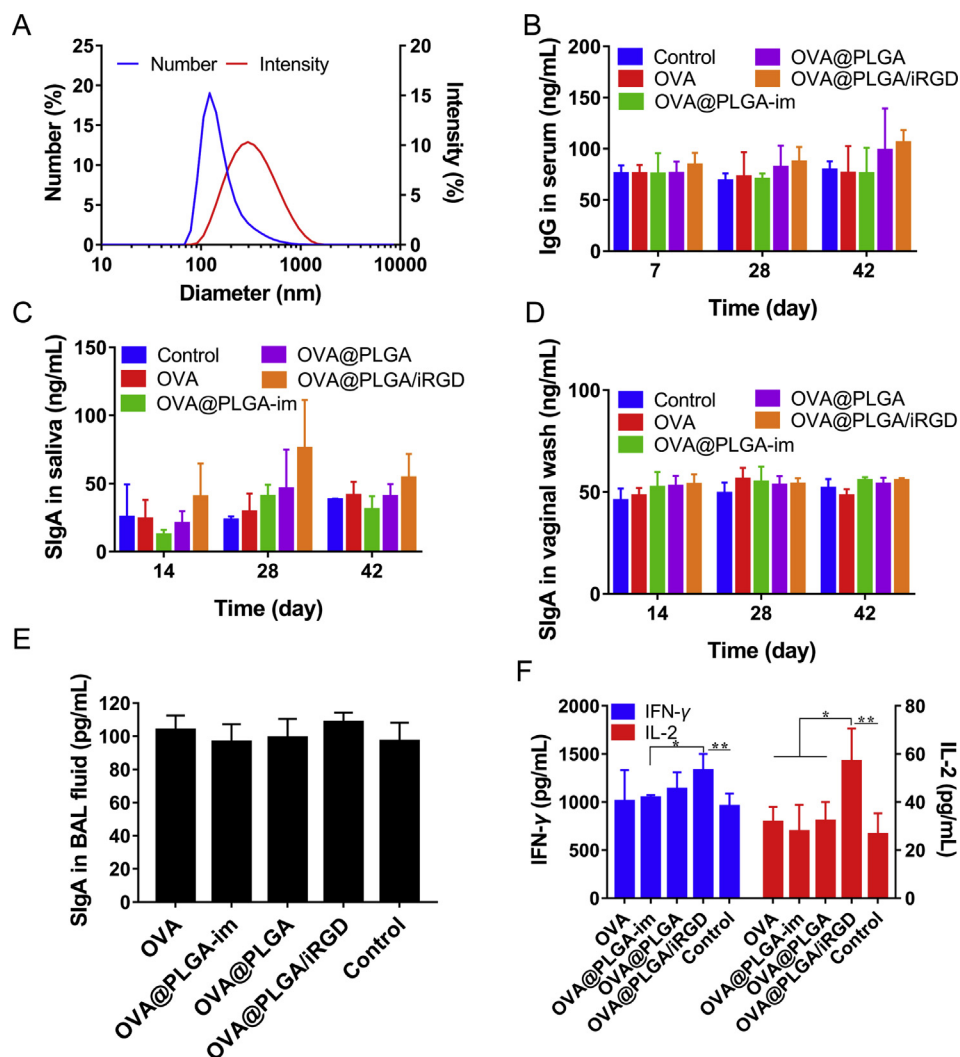


Figure 6 (A) Size distribution of OVA@PLGA by number and intensity. The rats were immunized on Days 0 and 14. (B) Determination of OVA specific IgG in serum at Days 7, 28 and 42 after administration of different preparations. Mucosal immune response was evaluated after 2 doses of formulation on Days 0 and 14. Secretory IgA (sIgA) levels were measured in (C) salivary secretion and (D) vaginal wash. (E) In addition, sIgA of bronchoalveolar lavage (BAL) fluid at the end of immunization was determined. The levels of (F) IFN- γ and IL-2 in spleen homogenates of rats at Day 42 after the first dose of the formulations (mean \pm SD, $n = 3-8$, * $P < 0.05$, ** $P < 0.01$).

response at distal organs may be due to the low immunogenicity of antigens. It needs the incorporation of immune adjuvant to get better effect in practical application. The same situation occurred in determination of sIgA levels in the bronchoalveolar lavage (Fig. 6E).

The mucosal immune response is divided into Th1 and Th2 types driven by different antigen types or adjuvants. The production of antibody is mainly mediated by Th2 immune response, and Th1 immune response mediates cellular immunity with production of IFN- γ and IL-2. After 42 days, the concentration of cytokines including IFN- γ and IL-2 in spleen homogenate was measured (Fig. 6F). In the measurement of IFN- γ concentration, there was not much difference between control group and plain OVA or OVA@PLGA-im group. In OVA@PLGA group, the concentration was 1.18-fold higher than the control group. In addition, the concentration of OVA@PLGA/iRGD group increased further to 1.34 times of the control group. In the

detection of IL-2, more obvious outcome displayed. The level of IL-2 in OVA@PLGA/iRGD was greatly improved to 1.77 times of the OVA@PLGA group. Taken together, the intranasal administration of OVA@PLGA could induce the immune response. Th2 and Th1 type immune responses were further enhanced after the combination of iRGD, which showed the increase of sIgA and IgG secretion, and the increase of IL-2 and IFN- γ secretion. It indicated that the uptake of nanoparticles increased after targeting M cells, which resulted in more effective immune response.

4. Conclusions

In this study, we co-cultured Calu-3 cells and Raji cells to construct an *in vitro* M-cell model that can be used to simulate the nasal cavity. Through co-culture of Calu-3 and Raji cells, a tightly connected monolayer was formed and M cells were induced to

differentiate. The differentiation of M cells increased the nanoparticle transportation efficiency of membrane. At the same time, the transport of nanoparticles was further enhanced after targeting M cells by iRGD. In addition, the systemic immune effect was enhanced, and a more advantageous mucus immunity was produced *in vivo*. The study provides a more nasal-like alternative to current M-cell model *in vitro*, and some insights into how to enhance the therapeutic effect of nasal administration by targeting M cells.

Acknowledgments

The work was supported by National Natural Science Foundation of China (81603057), Research Funds of Sichuan Science and Technology Department (2019YJ0048 and 19YYJC2250, China), the Fundamental Research Funds for the Central Universities (China), and 111 Project (B18035, China).

Author contributions

Xiaotong Yang, Xianchun Chen, Ting Lei, Lin Qin, Chuan Hu, Yang Zhou were mainly responsible for experimental design, data acquisition and analysis, and paper writing. Huile Gao and Qingfeng Liu put forward the hypothesis, supervised and guided experiments, reviewed and approved the manuscript for publication.

Conflicts of interest

The authors declare no conflict of interest.

References

- Türker S, Onur E, Ózer Y. Nasal route and drug delivery systems. *Pharm World Sci* 2004;**26**:137–42.
- Khan AR, Liu M, Khan MW, Zhai G. Progress in brain targeting drug delivery system by nasal route. *J Contr Release* 2017;**268**:364–89.
- Gao H. Progress and perspectives on targeting nanoparticles for brain drug delivery. *Acta Pharm Sin B* 2016;**6**:268–86.
- Li C, Wang J, Wang Y, Gao H, Wei G, Huang Y, et al. Recent progress in drug delivery. *Acta Pharm Sin B* 2019;**9**:1145–62.
- Zhou X, Hao Y, Yuan L, Pradhan S, Shrestha K, Pradhan O, et al. Nano-formulations for transdermal drug delivery: a review. *Chin Chem Lett* 2018;**29**:1713–24.
- Park J, Seo KW, Kim SH, Lee HY, Kim B, Lim CW, et al. Nasal immunization with M cell-targeting ligand-conjugated ApxIIA toxin fragment induces protective immunity against *Actinobacillus pleuropneumoniae* infection in a murine model. *Vet Microbiol* 2015;**177**:142–53.
- Lycke N. Recent progress in mucosal vaccine development: potential and limitations. *Nat Rev Immunol* 2012;**12**:592–605.
- Wang J, Wang Y, Zhang E, Zhou M, Lin J, Yang Q. Intranasal administration with recombinant *Bacillus subtilis* induces strong mucosal immune responses against pseudorabies. *Microb Cell Factories* 2019;**18**:103.
- Kiyono H, Fukuyama S. NALT-versus PEYER'S-patch-mediated mucosal immunity. *Nat Rev Immunol* 2004;**4**:699–710.
- Bernocchi B, Carpentier R, Betbeder D. Nasal nanovaccines. *Int J Pharm* 2017;**530**:128–38.
- Hagenaars N, Mastrobattista E, Verheul RJ, Mooren I, Glansbeek HL, Heldens JG, et al. Physicochemical and immunological characterization of *N,N,N*-trimethyl chitosan-coated whole inactivated influenza virus vaccine for intranasal administration. *Pharm Res (N Y)* 2009;**26**:1353–64.
- Ichinohe T, Tamura SI, Kawaguchi A, Ninomiya A, Imai M, Itamura S, et al. Cross-protection against H5N1 influenza virus infection is afforded by intranasal inoculation with seasonal trivalent inactivated influenza vaccine. *J Infect Dis* 2007;**196**:1313–20.
- Fan X, Su Q, Qiu F, Yi Y, Shen L, Jia Z, et al. Intranasal inoculate of influenza virus vaccine against lethal virus challenge. *Vaccine* 2018;**36**:4354–61.
- Dimova S, Brewster ME, Noppe M, Jorissen M, Augustijns P. The use of human nasal *in vitro* cell systems during drug discovery and development. *Toxicol Vitro* 2005;**19**:107–22.
- Gonçalves VS, Matias AA, Poejo J, Serra AT, Duarte CM. Application of RPMI 2650 as a cell model to evaluate solid formulations for intranasal delivery of drugs. *Int J Pharm* 2016;**515**:1–10.
- Kreft ME, Jerman UD, Lasič E, Rižner TL, Hevir-Kene N, Peternel L, et al. The characterization of the human nasal epithelial cell line RPMI 2650 under different culture conditions and their optimization for an appropriate *in vitro* nasal model. *Pharm Res (N Y)* 2015;**32**:665–79.
- Lin SF, Jiang PL, Tsai JS, Huang YY, Lin SY, Lin JH, et al. Surface assembly of poly(I:C) on polyethyleneimine-modified gelatin nanoparticles as immunostimulatory carriers for mucosal antigen delivery. *J Biomed Mater Res B Appl Biomater* 2019;**107**:1228–37.
- Lamichhane A, Azegami T, Kiyono H. The mucosal immune system for vaccine development. *Vaccine* 2014;**32**:6711–23.
- Fujimura Y. Evidence of M cells as portals of entry for antigens in the nasopharyngeal lymphoid tissue of humans. *Virchows Arch* 2000;**436**:560–6.
- Mabbutt NA, Donaldson DS, Ohno H, Williams IR, Mahajan A. Microfold (M) cells: important immunosurveillance posts in the intestinal epithelium. *Mucosal Immunol* 2013;**6**:666–77.
- Wang J, Gusti V, Saraswati A, Lo DD. Convergent and divergent development among M cell lineages in mouse mucosal epithelium. *J Immunol* 2011;**187**:5277–85.
- Kim SH, Seo KW, Kim J, Lee KY, Jang YS. The M cell-targeting ligand promotes antigen delivery and induces antigen-specific immune responses in mucosal vaccination. *J Immunol* 2010;**185**:5787–95.
- Des Rieux A, Ragnarsson EG, Gullberg E, Pr at V, Schneider YJ, Artursson P. Transport of nanoparticles across an *in vitro* model of the human intestinal follicle associated epithelium. *Eur J Pharmaceut Sci* 2005;**25**:455–65.
- Chaikhumwong P, Nilubol D, Tantivanont A, Chanvorachote P. A new cell-to-cell interaction model for epithelial microfold cell formation and the enhancing effect of epidermal growth factor. *Eur J Pharmaceut Sci* 2017;**106**:49–61.
- Zhuang J, Wang D, Li D, Yang Y, Lu Y, Wu W, et al. The influence of nanoparticle shape on bilateral exocytosis from Caco-2 cells. *Chin Chem Lett* 2018;**29**:1815–8.
- Des Rieux A, Fievez V, Th ate I, Mast J, Pr at V, Schneider YJ. An improved *in vitro* model of human intestinal follicle-associated epithelium to study nanoparticle transport by M cells. *Eur J Pharmaceut Sci* 2007;**30**:380–91.
- Beloqui A, Brayden DJ, Artursson P, Pr at V, Des Rieux A. A human intestinal M-cell-like model for investigating particle, antigen and microorganism translocation. *Nat Protoc* 2017;**12**:1387–99.
- Grainger CI, Greenwell LL, Lockley DJ, Martin GP, Forbes B. Culture of Calu-3 cells at the air interface provides a representative model of the airway epithelial barrier. *Pharm Res (N Y)* 2006;**23**:1482–90.
- Dong W, Ye J, Zhou J, Wang W, Wang H, Zheng X, et al. Comparative study of mucoadhesive and mucus-penetrative nanoparticles based on phospholipid complex to overcome the mucus barrier for inhaled delivery of baicalein. *Acta Pharm Sin B* 2019. Available from: <https://doi.org/10.1016/j.apsb.2019.10.002>.
- George I, Vranic S, Boland S, Courtois A, Baeza-Squiban A. Development of an *in vitro* model of human bronchial epithelial barrier to study nanoparticle translocation. *Toxicol Vitro* 2015;**29**:51–8.

31. Stentebjerg-Andersen A, Notlevsen IV, Brodin B, Nielsen CU. Calu-3 cells grown under AIC and LCC conditions: implications for dipeptide uptake and transepithelial transport of substances. *Eur J Pharm Biopharm* 2011;**78**:19–26.
32. Gupta PN, Khatri K, Goyal AK, Mishra N, Vyas SP. M-cell targeted biodegradable PLGA nanoparticles for oral immunization against hepatitis B. *J Drug Target* 2007;**15**:701–13.
33. Malik B, Goyal AK, Markandeywar TS, Rath G, Zakir F, Vyas SP. Microfold-cell targeted surface engineered polymeric nanoparticles for oral immunization. *J Drug Target* 2012;**20**:76–84.
34. Gullberg E, Leonard M, Karlsson J, Hopkins AM, Brayden D, Baird AW, et al. Expression of specific markers and particle transport in a new human intestinal M-cell model. *Biochem Biophys Res Commun* 2000;**279**:808–13.
35. Gullberg E, Keita ÅV, Salim SY, Andersson M, Caldwell KD, Söderholm JD, et al. Identification of cell adhesion molecules in the human follicle-associated epithelium that improve nanoparticle uptake into the Peyer's patches. *J Pharmacol Exp Therapeut* 2006;**319**:632–9.
36. Fievez V, Plapied L, Des Rieux A, Pourcelle V, Freichels H, Wascotte V, et al. Targeting nanoparticles to M cells with non-peptidic ligands for oral vaccination. *Eur J Pharm Biopharm* 2009;**73**:16–24.
37. Yoo MK, Kang SK, Choi JH, Park IK, Na HA, Lee HC, et al. Targeted delivery of chitosan nanoparticles to Peyer's patch using M cell-homing peptide selected by phage display technique. *Biomaterials* 2010;**31**:7738–47.
38. Roth-Walter F, Schöll I, Untersmayr E, Ellinger A, Boltz-Nitulescu G, Scheiner O, et al. Mucosal targeting of allergen-loaded microspheres by *Aleuria aurantia* lectin. *Vaccine* 2005;**23**:2703–10.
39. Garinot M, Fiévez V, Pourcelle V, Stoffelbach F, Des Rieux A, Plapied L, et al. PEGylated PLGA-based nanoparticles targeting M cells for oral vaccination. *J Contr Release* 2007;**120**:195–204.
40. Su H, Wang Y, Liu S, Wang Y, Liu Q, Liu G, et al. Emerging transporter-targeted nanoparticulate drug delivery systems. *Acta Pharm Sin B* 2019;**9**:49–58.
41. Hu C, Yang X, Liu R, Ruan S, Zhou Y, Xiao W, et al. Co-administration of iRGD with multistage responsive nanoparticles enhanced tumor targeting and penetration abilities for breast cancer therapy. *ACS Appl Mater Interfaces* 2018;**10**:22571–9.
42. Cun X, Chen J, Ruan S, Zhang L, Wan J, He Q, et al. A novel strategy through combining iRGD peptide with tumor-microenvironment-responsive and multistage nanoparticles for deep tumor penetration. *ACS Appl Mater Interfaces* 2015;**7**:27458–66.
43. Secott TE, Lin TL, Wu CC. *Mycobacterium avium* subsp. *paratuberculosis* fibronectin attachment protein facilitates M-cell targeting and invasion through a fibronectin bridge with host integrins. *Infect Immun* 2004;**72**:3724–32.
44. Yang X, Hu C, Tong F, Liu R, Zhou Y, Qin L, et al. Tumor microenvironment-responsive dual drug dimer-loaded PEGylated bilirubin nanoparticles for improved drug delivery and enhanced immune-chemotherapy of breast cancer. *Adv Funct Mater* 2019;**29**:1901896.
45. Thomas C, Rawat A, Hope-Weeks L, Ahsan F. Aerosolized PLA and PLGA nanoparticles enhance humoral, mucosal and cytokine responses to hepatitis B vaccine. *Mol Pharm* 2011;**8**:405–15.
46. Ramesh Babu PB, Chidekel A, Utidjian L, Shaffer TH. Regulation of apical surface fluid and protein secretion in human airway epithelial cell line Calu-3. *Biochem Biophys Res Commun* 2004;**319**:1132–7.
47. Lügering A, Floer M, Lügering N, Cichon C, Schmidt MA, Domschke W, et al. Characterization of M cell formation and associated mononuclear cells during indomethacin-induced intestinal inflammation. *Clin Exp Immunol* 2004;**136**:232–8.
48. Tyrer P, Ruth Foxwell FA, Kyd J, Harvey M, Sizer P, Cripps A. Validation and quantitation of an *in vitro* M-cell model. *Biophys Res Commun* 2002;**299**:377–83.
49. Brayden DJ, Jepson MA, Baird AW. Keynote review: intestinal Peyer's patch M cells and oral vaccine targeting. *Drug Discov Today* 2005;**10**:1145–57.
50. Yuki Y, Kiyono H. New generation of mucosal adjuvants for the induction of protective immunity. *Rev Med Virol* 2003;**13**:293–310.